Available online at www.sciencedirect.com
ScienceDirect
Journal of Power Sources 179 (2008) 50–59
JOURNAL OF POWER SOURCES
www.elsevier.com/locate/jpowsour

High surface area synthesis, electrochemical activity, and stability of tungsten carbide supported Pt during oxygen reduction in proton exchange membrane fuel cells

H. Chhina [a,b,*], S. Campbell [a], O. Kesler [b]

[a] *Automotive fuel cell corporation, 9000 Glenlyon Parkway, Burnaby, BC, Canada V5J 5J8*
[b] *Department of Mechanical and Industrial Engineering, 5 King's College Road, University of Toronto, Toronto, Ontario, Canada M5S 3G8*

Received 18 October 2007; received in revised form 14 December 2007; accepted 18 December 2007
Available online 6 January 2008

Abstract

The oxidation of carbon catalyst supports to carbon dioxide gas leads to degradation in catalyst performance over time in proton exchange membrane fuel cells (PEMFCs). The electrochemical stability of Pt supported on tungsten carbide has been evaluated on a carbon-based gas diffusion layer (GDL) at 80 °C and compared to that of HiSpec 4000™ Pt/Vulcan XC-72R in 0.5 M H_2SO_4. Due to other electrochemical processes occurring on the GDL, detailed studies were also performed on a gold mesh substrate. The oxygen reduction reaction (ORR) activity was measured both before and after accelerated oxidation cycles between +0.6 V and +1.8 V vs. RHE. Tafel plots show that the ORR activity remained high even after accelerated oxidation tests for Pt/tungsten carbide, while the ORR activity was extremely poor after accelerated oxidation tests for HiSpec 4000™. In order to make high surface area tungsten carbide, three synthesis routes were investigated. Magnetron sputtering of tungsten on carbon was found to be the most promising route, but needs further optimization.

Keywords: Catalyst support; Oxidation; Tungsten carbide; Carbon; Proton exchange membrane fuel cells; Electrocatalyst

1. Introduction

Proton exchange membrane fuel cells (PEMFCs) are electrochemical conversion devices used for power generation in portable, stationary, and transportation applications. PEMFCs in automotive applications are expected to experience up to 30,000 startup/shutdown cycles in their operating lifetime [1]. During startup, electrode potentials in excess of 1.5 V may be experienced for short periods of time, leading to a significant degradation in the fuel cell performance due to oxidation of the carbon catalyst support [1]. It is critical, therefore, to have a catalyst support that is more stable than carbon in PEMFCs.

Previously, studies have compared the stability of Pt supported on tungsten carbide with Pt supported on Vulcan XC-72R carbon [2]. Tungsten carbide is more stable than the carbon both under thermal oxidation and electrochemical oxidation conditions. Following the report by Levy and Boudart [3] about the electronic similarities between early transition metal carbides and noble metals, several investigations on the catalytic activity of carbides have been performed [4–11]. Meng and Shen [9,12,13] studied the effect of adding Pt onto tungsten carbides and observed a ten times larger activity on Pt–W_2C/C than on Pt/C for the oxygen reduction reaction (ORR) in an alkali medium, and proposed a synergy between the W_2C and the Pt; however, no mechanism for the synergy was proposed. Zellner and Chen [10] recently examined the electrochemical stability of WC and W_2C in acidic solutions and found that WC is stable in acid, although W_2C is not.

A major drawback preventing WC from being widely implemented in the catalyst industry, however, is the low surface area tungsten carbide produced by traditional metallurgical routes. Carbide preparation has been inherited from the metallurgical industry, where direct carburisation of WO_3, ammonium para tungstate, or ammonium meta tungstate with graphitic carbon at

* Corresponding author at: Automotive fuel cell corporation, Research Development, 9000 Glenlyon Parkway, Burnaby, BC, Canada V5J 5J8.
Tel.: +1 604 453 3834; fax: +1 604 453 3782.
E-mail address: harmeet.chhina@utoronto.ca (H. Chhina).

0378-7753/$ – see front matter © 2007 Elsevier B.V. All rights reserved.
doi:10.1016/j.jpowsour.2007.12.105

high temperatures (1400–1600 °C) is performed, leading to low specific surface area carbides [14,15]. This route usually produces mixed phase powders and excess free carbon, which may result in the formation of amorphous tungsten carbide phases [16]. Schmid and Roth [17] report that the less stable W_2C forms at temperatures below ~1200 °C, since the rate of diffusion is still too low to produce high concentrations of C in W. High temperatures are therefore typically required for synthesis of stable, stoichiometric WC. Synthesis of WC at lower temperatures in fewer hours is possible by using a gas–solid reaction between a W source and a carbon containing gas [17]. Koc and Kodambaka [15] developed a new method based on carbothermal reduction of novel carbon-coated precursors. They used tungsten trioxide as the tungsten precursor and used propane as the coating gas. Tungsten carbide formation is a diffusive process, occurring by the diffusion of carbon into tungsten [15]. Coated precursors produced high quality powders with single-phase, submicron WC at temperatures as low as 1100 °C. For temperatures greater than this, BET surface areas less than 20 $m^2\ g^{-1}$ were observed.

Carbides have been used previously as catalysts in fuel cells [5,7,8,18], but their use as catalyst supports has been rare. In one previous study, tungsten carbide supports with dispersed Pt were found to have high stability as determined both by thermogravimetric analysis and ex situ rotating disc electrode electrochemical tests at 30 °C [2]. In the current study, the ORR activity of Pt/WC and Pt/Vulcan XC-72R (a commercial carbon catalyst support) was determined both before and after accelerated oxidation cycles. Oxidation cycles between +0.6 V and +1.8 V were applied to the catalyst, and the activity of Pt dispersed on WC catalyst support was determined on a carbon-based gas diffusion layer (GDL) and on a gold mesh substrate at 80 °C in 0.5 M H_2SO_4. The commercial WC had a very low surface area (BET = 1.6 $m^2\ g^{-1}$) with an average crystallite size of 36 nm. The catalyst dispersion is controlled by the support surface area, and high catalyst dispersions lead to high catalyst activity [19]. Therefore, it is important to have a high surface area catalyst support. Alternative methods were studied to synthesize high surface area tungsten carbide. For fuel cell applications, a catalyst support material must have high surface area and be able to form agglomerates that have internal mesoporosity. Dense particles are therefore not preferred for use as a catalyst support. High surface area carbon was used as a template upon which tungsten was dispersed, which was later carburised to protect the carbon surface with WC. Here, synthesis procedures and characterization results are presented for WC synthesis on a high surface area carbon using three different routes: aqueous tungstate dispersion on carbon, an incipient wetness technique to disperse tungstate on carbon, and DC magnetron sputtering of tungsten on carbon.

2. Experimental procedure

The stability of tungsten carbide as a candidate material for use as a catalyst support was investigated by evaluating its stability in ex-situ electrochemical tests at 80 °C. Commercially available tungsten carbide powder (Alfa Aesar) was used in this study and 40 wt% Pt was deposited on the tungsten carbide. To obtain 40 wt% Pt on WC, 0.50 g of Pt(II) pentan-2,4-dionate was dissolved in 110 ml of acetonitrile. To this solution was added 0.36 g of Alfa Aesar WC. The solvent was allowed to evaporate and the resulting solid was heat treated in a tube furnace at 600 °C for 5 h under 20 vol.% H_2/balance Ar (0.23 SLPM).

X-ray diffraction (XRD) was used to determine the presence of crystalline Pt on the tungsten carbide catalyst support and the average crystallite size of each material. Crystallite sizes of the Pt and of the tungsten carbide were calculated using the Scherrer equation [20]:

$$t = \frac{0.9\lambda}{b\cos\theta_b} \quad (1)$$

where t is the crystallite size in Å, λ the wavelength (1.5406 Å in this case for Cu $K\alpha_1$ radiation), b the full-width at half maximum (FWHM) of a peak in the XRD spectrum, and θ_b is the diffraction angle for that peak.

Scanning electron microscopy (SEM) and transmission electron microscopy (TEM) were also used to characterize the microstructure of these materials.

To test the electrochemical stability of the catalyst supports, WC alone and 40 wt% Pt/WC were painted on a Ballard GDL. The powder and 33 wt% Nafion™ (DuPont, 850EW, 20 wt% in alcohol) solution were mixed and ~14 mg of the material was applied to a 6.5 cm^2 piece of Ballard GDL with a paint brush and dried on a hotplate. The electrode was then held with a gold wire, and a three-electrode electrochemical cell setup was used for electrochemical measurements. The electrochemical cell comprised a glass working compartment with a water jacket connected to a circulating water bath and two side compartments: one containing a Pt gauze counter electrode connected by a glass frit, and the other containing the reversible hydrogen electrode (RHE) connected by a Luggin capillary to which all potentials are referred. The electrode, held by a gold wire, was then immersed in deoxygenated 0.5 M H_2SO_4 at 30 °C or 80 °C.

To avoid the presence of background electrochemical signals from the underlying carbon gas diffusion paper in the GDL studies, gold mesh was also utilized as a substrate for additional tests to compare the results with those of the GDL studies. The supported catalyst material was mixed with Nafion™ (DuPont) solution and ~1.2 mg was applied on a gold mesh with a paintbrush. Based on previous voltage cycling experimental results, the oxidation potential chosen for the electrochemical cycling tests was +1.8 V vs. RHE [21]. At lower potentials, the oxidation was not detectable in the experimental timeframe. Oxidation cycling was performed using an EG&G 263 (PAR, Princeton, NJ) potentiostat with Corrware software (Scribner Associates). Potential steps between +0.6 V and +1.8 V were applied between 60 s holds at +0.6 V and 20 s holds at +1.8 V. Cyclic Voltammograms (CVs) were recorded between 0.0 V and +1.4 V at 100 mV s^{-1} both before the oxidation cycles began and then again after every 10 oxidation cycles, until a total of 100 oxidation cycles had been applied. Observations were made of changes in ORR activity after oxidation cycles by measuring ORR activity both before and after the oxida-

tion cycles. HiSpec 4000™ (Johnson Matthey, U.K., 40 wt% Pt/Vulcan XC-72R) was tested using the same procedure for comparison.

Thermogravimetric analysis (TGA) was used to determine the content of W sputtered on carbon by DC magnetron sputtering. The sample was held at 50 °C for 5 min to allow time for water removal. The samples were held in air (40 ml min^{-1}) and the temperature was ramped from 50 °C to 1000 °C at 2 °C min^{-1}.

In order to enhance the electrochemical activity of the Pt/WC support catalyst, three techniques were developed to produce higher surface area WC support on which Pt could be more finely dispersed. High surface area carbon was used as a template upon which tungsten was dispersed by an aqueous tungstate reduction method, an incipient wetness method, and by DC magnetron sputtering. The dispersed W on carbon mixtures were then heat treated in a tube furnace under Ar/H_2 atmospheres. Several molar ratios of W:C were investigated in order to determine the optimal tungsten loading for each technique investigated.

2.1. Aqueous dispersion of tungstate on carbon followed by reduction to tungsten carbide

In order to make a 1:4 W:C molar ratio mixture, one gram of Vulcan XC-72R (Cabot) was added to 50 ml water, which was then boiled. Separately, 5.14 g of ammonium paratungstate (APT) was dissolved in 100 ml of water (18.2 MΩ) at 65 °C. The APT solution was added to the carbon/water mixture, and to this was added 0.27 mol of $NaBH_4$ dissolved in 100 ml water. The resulting mixture bubbled vigorously, had a pH of 9, and had a brown-black appearance. The mixture was allowed to equilibrate for approximately 15 min until the bubbling stopped. Then 0.5 M H_2SO_4 acid was added until a pH between 5 and 6 was obtained. This mixture was left overnight to settle.

The next day, a gradient of solution color from a green-brown solution near the surface to a pale blue solution closer to the solids at the bottom of the beaker was observed. The green-brown solution was decanted off. The pH of the pale blue solution closer to the solids was approximately 4. To the pale-blue solution, a small amount of 0.5 M sulfuric acid was added to observe any change with acid addition. There was no precipitate observed in this solution, and it turned clear after leaving it at room temperature overnight. The solid tungsten deposited on carbon material was then filtered (Whattman 541 hardened ashless filter paper, 90 mm), washed, dried on a hotplate for 5 h, and ground. The W/C material was heat-treated at 1100 °C for 10 h in 20% H_2/balance Ar.

2.2. Incipient wetness

A mixture of 0.5 g of carbon in 50 ml water was heated at 85 °C and to this was added 5.6 g of APT dissolved in 150 ml water. The mixture was then heated at 100 °C to evaporate the water. A mixture of black and white powder resulted after all of the water had evaporated. The ground powder of this mixture was heated at 1100 °C for 10 h in 20% H_2/balance Ar.

2.3. DC magnetron sputtering of W onto C

Carbon powder (Vulcan XC-72 R) was sputter-coated with tungsten with the use of a 5 cm diameter planar magnetron. The distance between the powder and the sputter target was 10 cm. Prior to deposition, the chamber was pumped to 3×10^{-6} Torr with the use of an oil diffusion pump with a liquid nitrogen cold trap. The chamber pressure was elevated to 3×10^{-3} Torr during sputter operation by continuous throttled flow of argon into the chamber. A variable orifice plate was located between the cold trap and the diffusion pump, to keep the pressure at the inlet of the diffusion pump below 6×10^{-4} Torr. The carbon powder was agitated with the use of an ultrasonic driver in order to prevent the powder from clumping together and to expose the entire surface of each grain to the sputtered flux. DC power of 80 W was applied to the magnetron with the use of an Advanced Energy MDX1K power supply. The W/C material produced was heat-treated at 1100 °C for 10 h under 20% H_2/balance Ar.

3. Results and discussion

3.1. Electrochemical testing

Oxidation of carbon-supported catalyst at high potential causes loss of Pt activity as a result of Pt particle detachment from the carbon support, oxidation of the carbon, and thick Pt oxide formation [22]. Carbon support oxidation causes Pt to fall off the catalyst support, making the Pt irreversibly inactive. Pt oxide, however, is reduced when the voltage is stepped to 0.6 V, thus making the voltage cycling suitable for isolating the effect of carbon oxidation on the electrochemical performance degradation, while minimizing the contribution of the growth of a Pt oxide layer. The current was measured as the electrode was cycled between +0.6 V and +1.8 V (Fig. 1). Oxygen reduction reaction activity was measured both before and

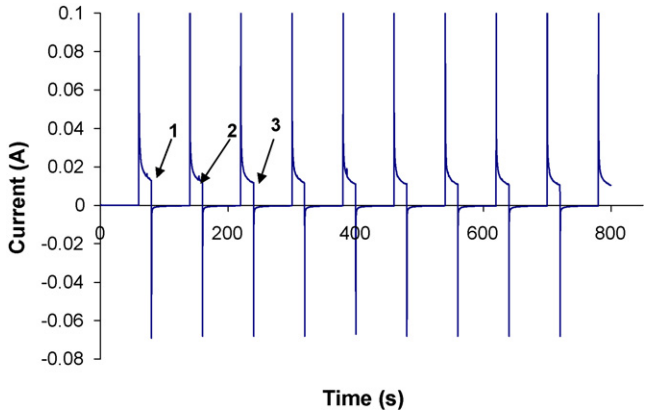

Fig. 1. Current response to oxidation cycles of 40 wt% Pt/WC between +0.6 V and +1.8 V in 0.5 M H_2SO_4, at 80 °C with bubbled N_2. Points 1, 2, 3, etc. were used to calculate the normalized activity.

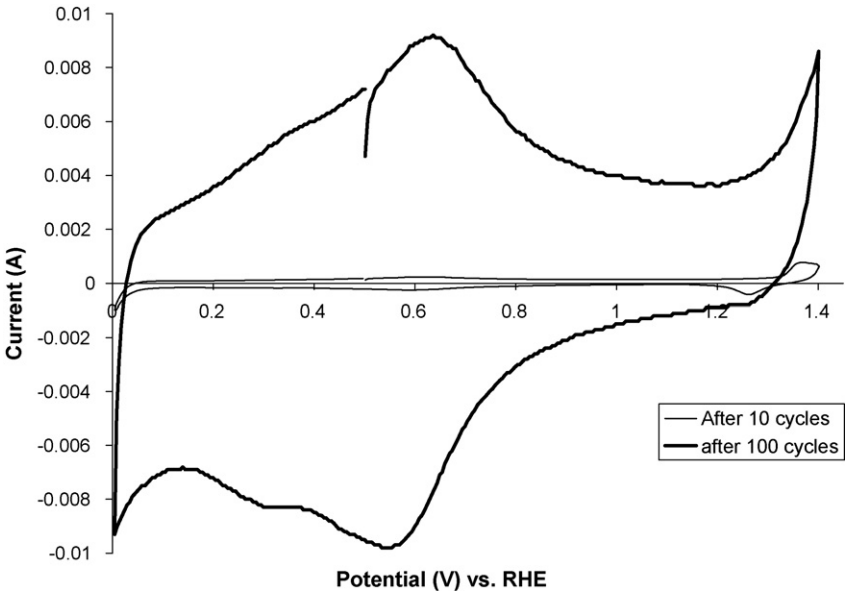

Fig. 2. Cyclic voltammogram of the gas diffusion layer (carbon fiber paper with carbon sublayer), in 0.5 M H_2SO_4, at 80 °C with bubbled N_2.

after a series of oxidation cycles from +0.6 V to +1.8 V. Cyclic voltammograms (CV) were also recorded in order to determine the loss in Pt surface area resulting from the oxidation cycles.

An increase in capacitance with time was observed for cyclic voltammograms of tungsten carbide with Nafion coated on a GDL both before and after oxidation cycles at 80 °C, both with and without Pt catalyst for comparison. Anodic and cathodic peaks were observed at ~0.58 V and ~0.65 V, respectively, for both WC painted alone on a GDL and for 40 wt% Pt/WC painted on a GDL. In order to determine whether these peaks resulted from an unknown species formed on the surface of tungsten carbide or on the surface of the underlying carbon fiber paper, the GDL was also cycled alone. The CVs for the underlying carbon fiber paper (Fig. 2) showed a significant increase in current after 100 oxidation cycles. Reversible species were observed at 0.58 V and at 0.65 V, which result from surface oxidation of the carbon on the GDL, forming quinone/hydroquinones on the GDL surface [23].

In order to avoid interference from the electrochemical activity of the GDL substrate, gold mesh was also used as a substrate to study the stability of Pt/WC in order to observe whether there was any loss in the ORR activity after the oxidation cycles for these materials. The ORR activity was observed both before and after the oxidation cycles. Fig. 1 shows oxidation cycle data for 40 wt% Pt on WC cycled from +0.6 V to +1.8 V. These data were used to calculate the normalized activity of Pt supported on tungsten carbide cycled at 80 °C in Fig. 3. The normalized activity was calculated by recording the last current point from the data set at 1.8 V in the oxidation cycles just before the current became negative under +0.6 V conditions. These points are marked with arrows as points 1, 2, 3, etc. in Fig. 1. The current at point 1 was taken as the initial current for the normalized activity plots. The current decreased as the catalyst support oxidized, so the currents subsequent to point 1 were normalized to the initial current value, and the curve in Fig. 3 was plotted as the normalized activity vs. the cumulative number of oxidation cycles. Tafel plots showing the ORR activity both before and after oxidation cycles at 80 °C of 40 wt% Pt/WC (Fig. 4) and HiSpec 4000^{TM} (Fig. 5) show significantly higher stability of the Pt/WC catalyst. The open circuit potential (OCP) was higher after oxidation cycles for Pt/WC. The higher OCP after the oxidation cycles may have resulted from activation of Pt that initially might have been covered with carbon from the organics in the Pt precursor. Since Pt(II) pentan-2,4-dionate was used as the Pt precursor and the Pt was later reduced in an Ar/H_2 atmosphere, the organics from the precursor may have covered the Pt. Those organics would then have oxidized upon application of the oxidation cycles from +0.6 V to +1.8 V, leading to a cleaner Pt surface and thereby increasing the Pt activity.

The catalytic activity of Pt/C was observed to degrade rapidly with the oxidation cycling, as determined both by the ORR activ-

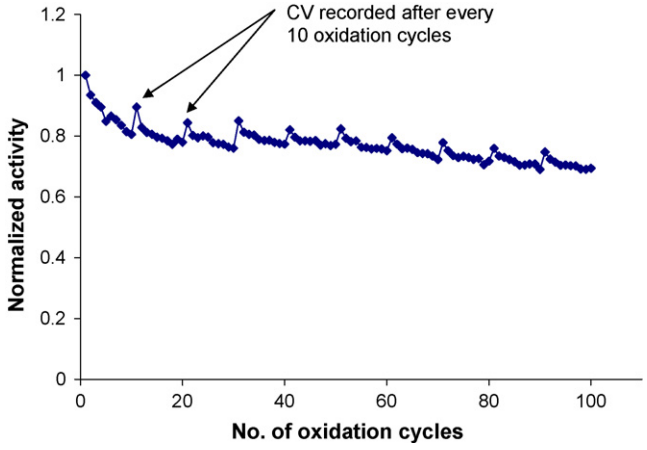

Fig. 3. Normalized activity of 40 wt% Pt/WC painted on a gold mesh in 0.5 M H_2SO_4, at 80 °C with bubbled N_2.

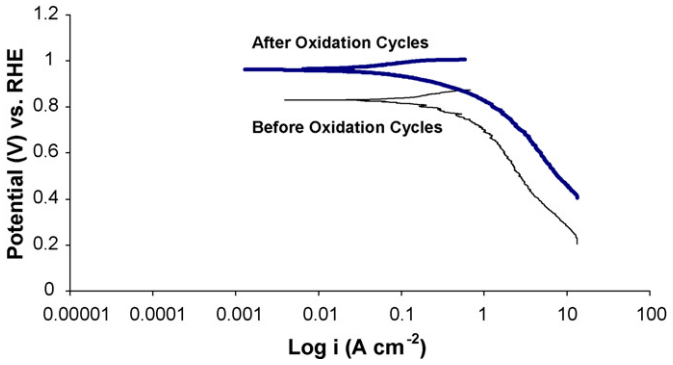

Fig. 4. Tafel plots of 40 wt% Pt/WC painted on a gold mesh in 0.5 M H_2SO_4, at 80 °C with bubbled O_2. Average of five tests is plotted. Thin line: ORR activity before oxidation cycles. Thick line: ORR activity after 100 oxidation cycles.

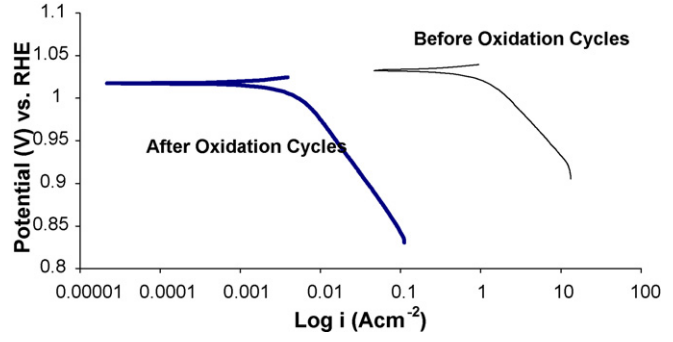

Fig. 5. Tafel plot of HiSpec 4000™ painted on a gold mesh in 0.5 M H_2SO_4, at 80 °C with bubbled O_2. Average of five tests is plotted. Thin line: ORR activity before oxidation cycles. Thick line: ORR activity after 100 oxidation cycles.

ity measurements on the gold mesh as well as in the cyclic voltammetry tests performed after every 10 cycles. The cyclic voltammetry results for 40 wt% Pt/WC (Fig. 6) compared to those for HiSpec 4000™ (Fig. 7) show that 40 wt% Pt/WC is stable even after 100 oxidation cycles, while HiSpec 4000™ lost its entire Pt oxide reduction peak (~0.75 V) after 100 oxidation cycles. The increase in the hydrogen adsorption/desorption peak area observed for the Pt/WC CV (Fig. 6) has also been reported by other researchers [24,25]. Cycling between +0.6 V and +1.8 V may cause tungsten carbide to oxidize to tungsten oxide. Tungsten oxide, by reacting with hydrogen, can form two stable hydrogen tungsten bronzes, $H_{0.18}WO_3$ and $H_{0.35}WO_3$, or sub-stoichiometric tungsten oxides [24,25]. Since tungsten oxide exhibits fairly high electrochemical stability [26], its formation is less deleterious to the electrochemical performance of the cell than the oxidation of a carbon catalyst support, which leads to irreversible platinum detachment and corresponding complete activity loss.

From the electrochemical tests performed, tungsten carbide appears to be a much more stable catalyst support at 80 °C compared to carbon for PEMFCs. The lower catalytic activity observed in these tests might result from the lower surface area of the commercial carbide (1.6 $m^2\,g^{-1}$) compared to the high surface area of the carbon catalyst support (250 $m^2\,g^{-1}$) used for HiSpec 4000™, as well as from differences in the catalytic activity of the catalyst/support material combinations. In order to better isolate the contributions of the material composition from that of the microstructure, new synthesis routes were developed to produce higher surface area WC catalyst supports in order to improve the overall catalytic performance. The optimized particle size distribution of the catalyst and support particles still needs to be established in order to achieve the required electrochemical activity.

3.2. Characterization of high surface area tungsten carbide

3.2.1. Aqueous dispersion of tungstate on carbon followed by reduction to tungsten carbide

An XRD pattern for 1:4 W:C molar ratio-based WC synthesized by aqueous dispersion of tungstate is shown in Fig. 8. XRD peaks corresponding to W, WC, and W_2C are present. Even though tungstate was successfully deposited onto the carbon, the majority of the tungstate remained dissolved in water; therefore, the yield of tungsten carbide from this solution was

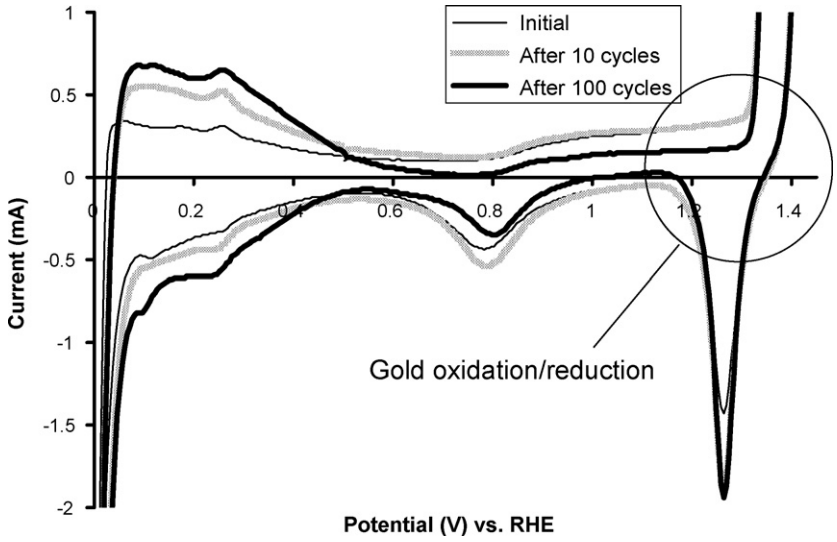

Fig. 6. Cyclic voltammogram of 40 wt% Pt/WC painted on a gold mesh in 0.5 M H_2SO_4, at 80 °C with bubbled N_2.

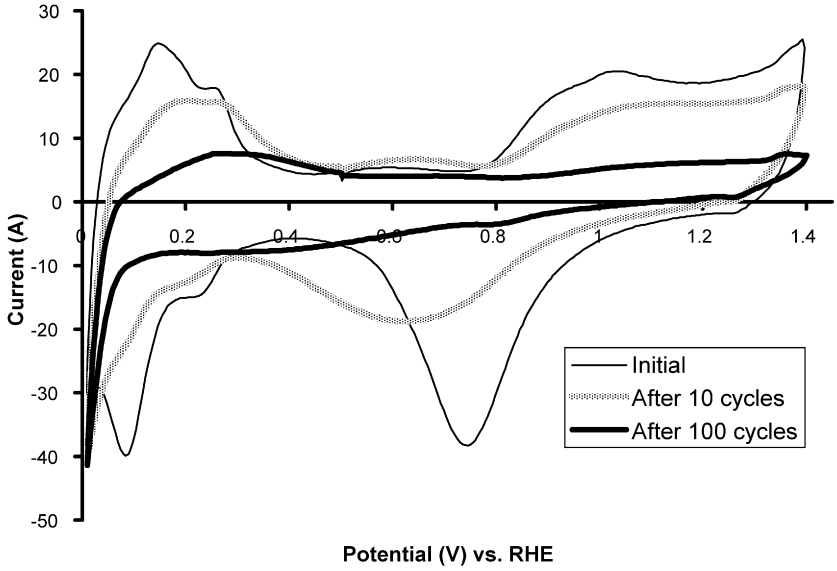

Fig. 7. Cyclic voltammogram of HiSpec 4000™ painted on a gold mesh in 0.5 M H_2SO_4, at 80 °C with bubbled N_2.

extremely poor. Several parameters including temperature, pH, amount of water addition, and use of formaldehyde (as a mild reducing agent) were varied to determine their effect on the ability to reduce the tungstate to tungsten directly on the surface of carbon. However, none of these parameters had any significant effect on the reduction of the tungstate onto the carbon.

The aqueous technique to disperse tungsten onto carbon was therefore abandoned due to the low yield (10%) of the tungstate deposition onto carbon. The formation of polytungstates [27] may have decreased the yield of this process. For tungsten in the pH range of 5–7.8, the equilibrium involves the formation of WO_4^{2-}, $W_6O_{20}(OH)_2^{6-}$, $HW_7O_{24}^{5-}$, and $H_2W_{12}O_{42}^{10-}$ [27]. Anderson and Bergstrom [28] report that W(VI) forms a number of different polynuclear species in solution. The formation of several tungstates in aqueous solution makes the chemistry of this material quite complex, so non-aqueous routes and routes involving a minimal change in pH were also examined.

3.2.2. Incipient wetness

An XRD pattern for a mixture of tungsten and carbon in a 1:3 W:C molar ratio sample formed by the incipient wetness technique (Fig. 9) shows the presence of WC alone. The presence of both W_2C and WC is observed for the 1:1 W:C molar ratio sample, and both W and W_2C are observed for the 3:1 W:C molar ratio samples in addition to WC. An optimum amount of W therefore needs to be dispersed in order to achieve the stoichiometric WC phase alone. Table 1 shows the XRD crystallite size of WC formed both by incipient wetness and magnetron sputtering. For the 1:3 W:C molar ratio sample, a crystallite size of 17.6 nm was calculated using the 2θ peaks at 31.48°, 35.66°, and 48.27°. For the 1:1 W:C molar ratio sample, a WC

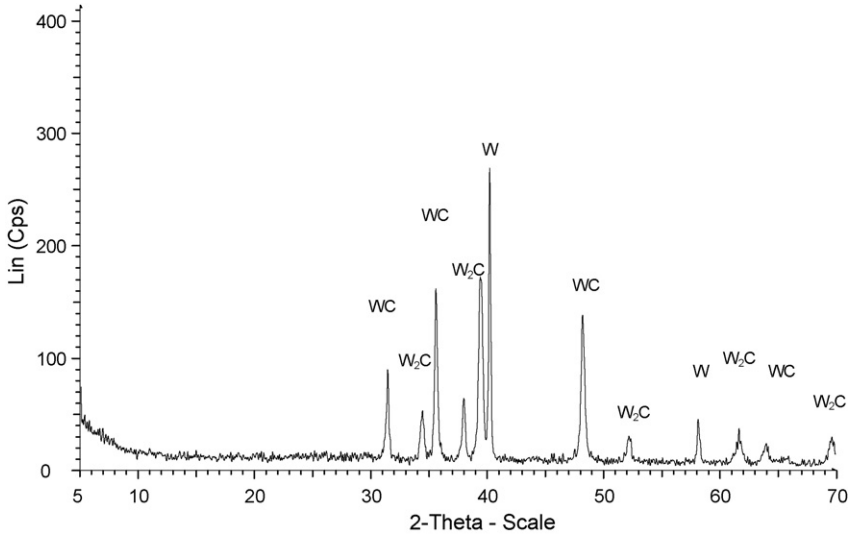

Fig. 8. XRD spectrum of a 1:4 W:C molar ratio mixture formed by aqueous dispersion of reduced tungstate onto carbon, followed by heat treatment at 1150 °C for 10 h under 20% H_2/balance Ar.

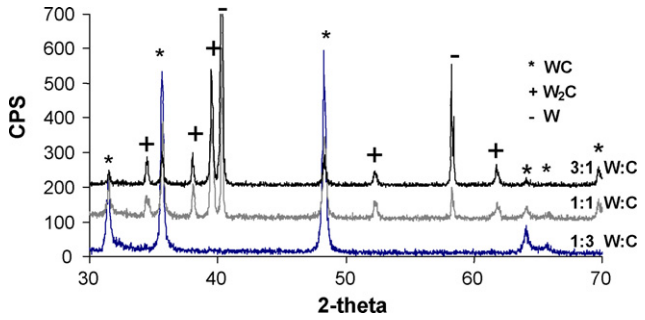

Fig. 9. XRD spectrum of heat-treated 1:3, 1:1, and 3:1 W:C mole ratios of W deposited on Vulcan XC-72R C by incipient wetness, followed by heat treatment at 1100 °C for 10 h under 20 vol.% H_2/balance Ar.

Table 1
XRD crystallite size of WC formed by both incipient wetness and DC magnetron sputtering

Materials	WC crystallite size
1:3 W:C molar ratio by incipient wetness	17.6
1:1 W:C molar ratio by incipient wetness	37.3
WC produced by DC magnetron sputtering	21.3

crystallite size of 37.3 nm was calculated using the same 2θ peaks.

An SEM micrograph (Fig. 10) of the 1:3 W:C molar ratio sample shows the presence of areas with crystalline WC, and areas with bare carbon. The presence of C alone is not preferred, because it will oxidize under fuel cell potential excursions during startup/shutdown. For the 1:1 W:C molar ratio sample and 3:1 W:C molar ratio sample, crystalline facets with very little bare carbon are observed, although the crystallite sizes of the WC particles are larger than those formed in the 1:3 W:C ratio mixture. TEM images of the same material (Fig. 11) show individual WC particles supported on carbon. Some of the individual particles are approximately 1 μm in diameter, with agglomerates ranging from 5 μm to 9 μm. The agglomerates appear dense, with little or no mesoporosity.

Table 2
BET measurement of Vulcan XC-72R and of WC made by incipient wetness

Material	BET surface area ($m^2\ g^{-1}$)
Vulcan XC-72R	252.13
1:3 molar W:C WC by incipient wetness	41.15
1:1 molar W:C WC by incipient wetness	12.74
3:1 molar W:C WC by incipient wetness	0.613

Catalyst supports with particle sizes ranging from 50 nm to 100 nm with agglomerates in the μm range that have internal porosity are typically used in PEMFCs. The WC particles produced in this study by incipient wetness have low surface area (Table 2), and agglomerates ranging from 5 μm to 9 μm are not preferred because polymer electrolyte membranes as thin as 25 μm are used. The coarse WC particles may cause the membrane to be pinched, leading to the formation of a hole in the membrane under operation. Furthermore, carbon has a BET surface area of ~250 $m^2\ g^{-1}$, and WC materials produced via the incipient wetness route have significantly lower surface areas ranging from 0.613 $m^2\ g^{-1}$ for the 3:1 W:C molar ratio to 41.15 $m^2\ g^{-1}$ for the 1:3 W:C molar ratio sample. The BET data correlate well with the TEM images, in which less free carbon is observed with higher amounts of tungsten addition. The WC particles also appear dense, with little mesoporosity visible. Therefore, while this processing route did result in

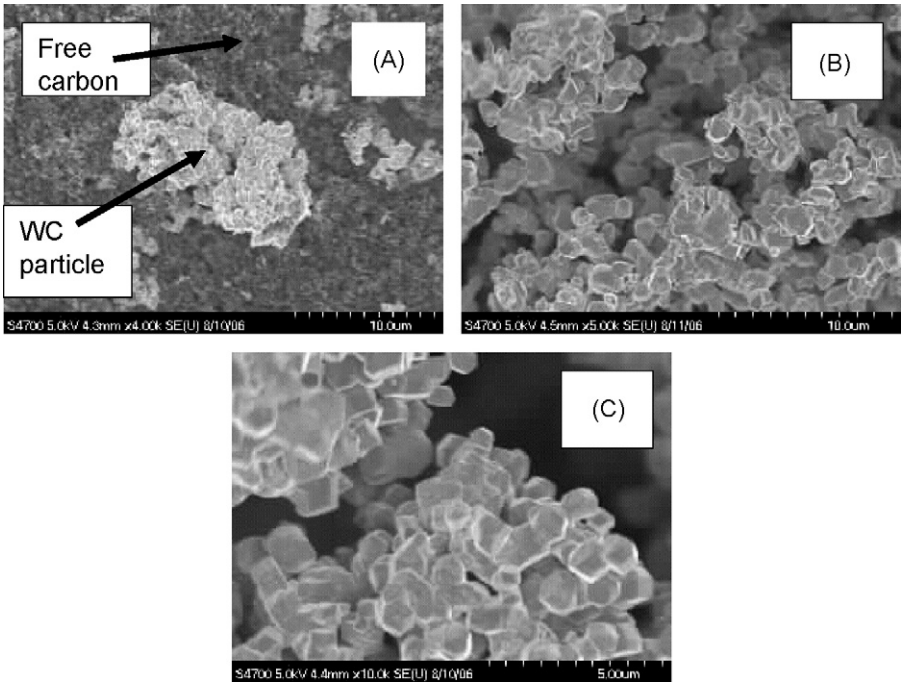

Fig. 10. SEM micrographs of heat-treated samples prepared via incipient wetness. (A) 1:3 W:C molar ratio, (B) 1:1 W:C molar ratio and (C) 3:1 W:C molar ratio.

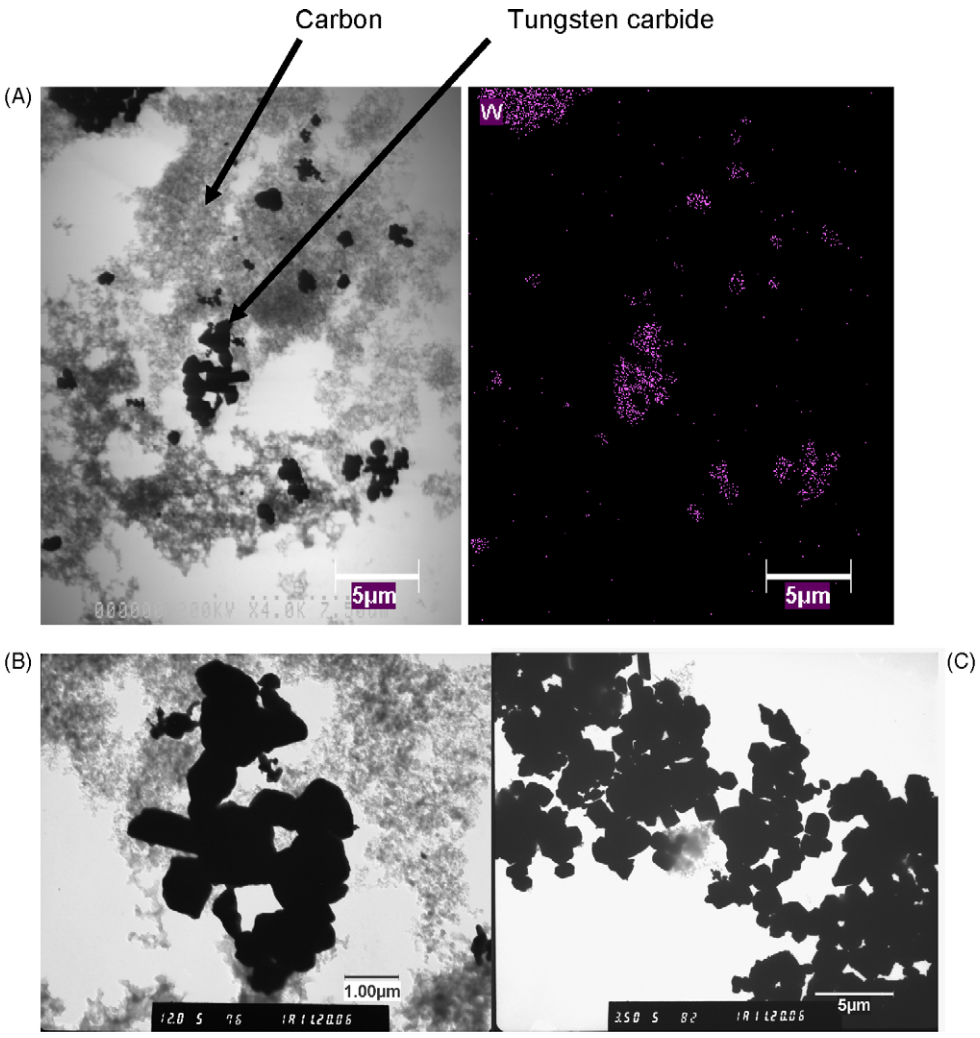

Fig. 11. TEM images of heat-treated samples prepared via incipient wetness. (A) 1:3 W:C molar ratio, (B) 1:1 W:C molar ratio and (C) 3:1 W:C molar ratio.

a higher yield of tungstate dispersion on carbon, the material formed still did not have a sufficiently high surface area for use in PEMFCs.

3.2.3. DC magnetron sputtering of W onto C

An XRD pattern for tungsten carbide synthesized by sputtering of W onto C followed by heat treatment at 1100 °C for 10 h under Ar/H_2 (80/20 vol.%) is shown in Fig. 12. The pattern shows the presence of a broad peak at 2θ of 24°, which corresponds to unreacted amorphous carbon. WC peaks are observed, from which a crystallite size of 21.3 nm is calculated (Table 1). From TGA data, it was calculated that 11 wt% of W is deposited on C (Fig. 13), which is very low considering the significant density difference between the two materials (with densities of 1.8 g cm^{-3} for C and 19 g cm^{-3} for W).

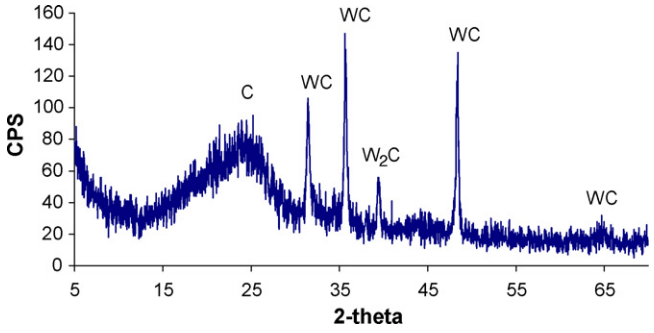

Fig. 12. XRD spectrum of W sputtered onto carbon by DC magnetron sputtering, followed by carbidization in a tube furnace at 1100 °C for 10 h under 20% H_2/balance Ar.

TEM images (Fig. 14) show formation of WC nanoparticles by DC magnetron sputtering. The particles in this case are not as dense as those observed in Fig. 11 prepared by incipient wetness. The agglomerates of WC have a similar morphology as the carbon on which the W was sputtered. Since sputtering allows the deposition of very small particles with sufficient porosity to separate them, the heat treatment to form the carbide phase did not lead to sintering of the particles as it did with the other two deposition techniques, which likely formed more closely packed W particles in the initial deposition stages, which then sintered further during carburization.

These results show that the production of high surface area WC is possible by the sputtering of W onto carbon, followed by carbidization. Some free carbon was observed in the mate-

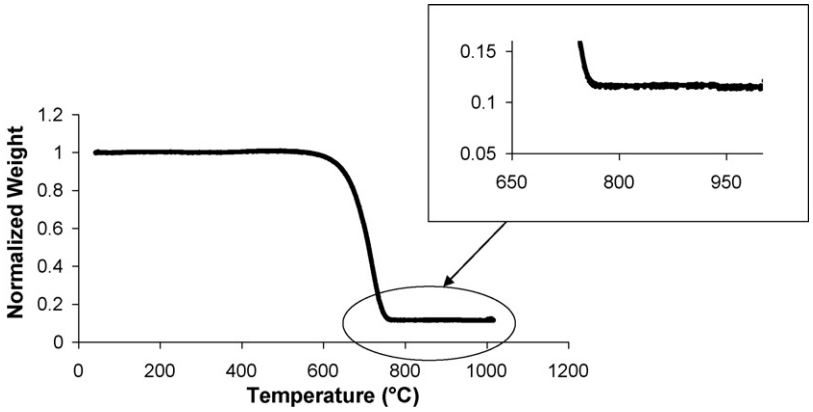

Fig. 13. TGA data of W sputtered on carbon. Temperature ramped from 50 °C to 1000 °C at 2 °C min^{-1} under air flowing at 40 ml min^{-1}.

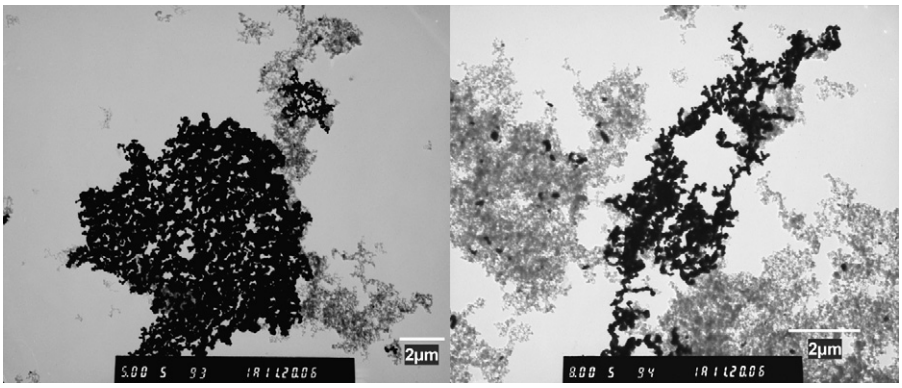

Fig. 14. TEM images of W sputtered onto Vulcan XC-72R and then heat-treated at 1100 °C for 10 h under 20% H_2/balance Ar.

rial produced by sputtering in this study, but optimization of the technique, including the length of sputtering time and, perhaps most importantly, the nature and extent of agitation of the powders, could lead to the production of pure WC nanoparticles with agglomerates that are in the μm range. The TEM microstructures showing agglomerates of nanoparticles with high mesoporosity suggest that sputtering may be a promising technique for producing high surface area WC with a morphology closely resembling that of the carbon catalyst supports used in PEMFCs. However, the sputtering method needs to be optimized to fully cover the carbon surface, most likely with the addition of a mechanism for more thorough agitation of the powder onto which the W is sputtered. A sputtering time of 4 h was used in this study, and increasing this time or changing the sputtering conditions may also allow better coverage of carbon with tungsten.

4. Conclusions

The oxygen reduction reaction (ORR) activity before and after oxidation cycles between +0.6 V and +1.8 V was studied for both Pt/tungsten carbide and for a commercial catalyst, HiSpec 4000^{TM}. Tafel plots showed that the Pt/tungsten carbide was stable even after 100 oxidation cycles, and sustained its high ORR activity at 80 °C, while the HiSpec 4000^{TM} lost its ORR activity much more rapidly. As an initial step toward increasing the baseline electrochemical activity of the Pt/WC, three synthesis techniques were investigated to produce higher surface area WC catalyst support. The synthesis of high surface area WC using the aqueous reduction technique led to a low yield (10%) of W deposition, and the incipient wetness technique led to the formation of dense WC particles with agglomerates of 5–9 μm. DC magnetron sputtering of W onto C, however, proved to be a promising technique for high surface area WC synthesis, leading to porous agglomerates that were not as dense as those obtained by either of the other two techniques. Optimization of the magnetron sputtering method is still needed to produce more uniform coverage of the C powder with W. The technique appears to lead to high surface area carbon protected by a WC surface coating, thus possibly allowing the benefits of high surface area and low density of carbon supports to be combined with the higher stability of the WC against surface oxidation. These results suggest that tungsten carbide may be a feasible candidate for use as a PEMFC catalyst support material with substantially improved oxidative stability.

Acknowledgement

The authors gratefully acknowledge Dr. Bob Parsons for help with tungsten sputtering on carbon.

References

[1] M. Mathias, R. Makharia, H. Gasteiger, J. Conley, T. Fuller, C. Gittleman, S. Kocha, D. Miller, C. Mittesteadt, T. Xie, S. Yan, P. Yu, Interface 14 (2005) 24–35.

[2] H. Chhina, S. Campbell, O. Kesler, J. Power Sources 164 (2007) 431–440.
[3] R.B. Levy, M. Boudart, Science 181 (1973) 547–549.
[4] M. Boudart, S.T. Oyama, L. Volpe, Board of Trustees of Leland Stanford Jr. University, 4,515,763, 4 A.D.
[5] J.B. Christian, R.G. Mendenhall, Osram Sylvania Inc., US6,656,870 B2, 1–9 (2003).
[6] A. Lofberg, L. Seyfried, P. Blehen, S. Decker, J.M. Bastin, A. Frennet, Catal. Lett. 33 (1995) 165–173.
[7] C. Ma, W. Zhang, D. Chen, B. Zhou, Trans. Nonferr. Met. Soc. Chin. 12 (2002) 1015–1019.
[8] C. Ma, Y. Gan, Y. Chu, H. Huang, D. Chen, B. Zhou, Trans. Nonferr. Met. Soc. Chin. 14 (2004) 11–14.
[9] H. Meng, P.K. Shen, Chem. Commun. (2005) 4408–4410.
[10] M.B. Zellner, J.G. Chen, J. Electrochem. Soc. 152 (2005) A1483–A1494.
[11] P. Zoltowski, Electrochim. Acta 25 (1980) 1547–1554.
[12] H. Meng, P.K. Shen, Electrochem. Commun. 8 (2006) 588–594.
[13] H. Meng, P.K. Shen, J. Phys. Chem. B 109 (2005) 22705–22709.
[14] C. Liang, F. Tian, Z. Li, Z. Feng, Z. Wei, C. Li, Chem. Mater. 15 (2003) 4846–4853.
[15] R. Koc, S.K. Kodambaka, J. Eur. Ceram. Soc. 20 (2000) 1859–1869.
[16] N. Radic, B. Pivac, F. Meinardi, Koch, Mater. Sci. Eng. A 396 (2005) 290–295.
[17] K. Schmid, J. Roth, J. Nucl. Mater. 302 (2002) 96–103.
[18] J.B. Christian, T.A. Dang, R.G. Mendenhall, Osram Sylvania Inc., US6,551,569 B1, 1–9, 3 A.D.
[19] K. Kinoshita, Carbon: Electrochemical and Physicochemical Properties, John Wiley and Sons Inc., 1988.
[20] B.D. Cullity, Elements of X-Ray Diffraction, Addison Wesley Publishing Company Inc., 1978, pp. 1–30.
[21] H. Chhina, S. Campbell, O. Kesler, J. Power Sources 161 (2006) 893–900.
[22] Y.F. Yang, G. Denault, J. Electroanal. Chem. 443 (1998) 273–282.
[23] K. Kangasniemi, D. Condit, T. Jarvi, J. Electrochem. Soc. 151 (2004) E125–E132.
[24] J. Shim, C.R. Lee, H.K. Lee, J.S. Lee, E.J. Cairns, J. Power Sources 102 (2001) 172–177.
[25] P.J. Kulesza, L.R. Faulkner, J. Electrochem. Soc. 136 (1989) 707–713.
[26] H. Chhina, S. Campbell, O. Kesler, J. Electrochem. Soc. 164 (6) (2007) B533–B539.
[27] A. Cotton, G. Wilkinson, Advanced Inorganic Chemistry, John Wiley and Sons Inc., 1988, pp. 808–812.
[28] K.M. Andersson, L. Bergstrom, Int. J. Refract. Met. Hard Mater. 18 (2000) 121–129.